01 Jan 2010

Direct Numerical Simulation Of Hypersonic Turbulent Boundary Layers With Varying Freestream Mach Number

L. (Lian) Duan
Missouri Unviersity of Science and Technology, duanl@mst.edu

I. Beekman

M. P. Martin

Recommended Citation

L. Duan et al., "Direct Numerical Simulation Of Hypersonic Turbulent Boundary Layers With Varying Freestream Mach Number," *48th AIAA Aerospace Sciences Meeting Including the New Horizons Forum and Aerospace Exposition*, article no. 2010-0353, American Institute of Aeronautics and Astronautics, Jan 2010.
The definitive version is available at https://doi.org/10.2514/6.2010-353

48th AIAA Aerospace Sciences Meeting Including the New Horizons Forum and Aerospace Exposition
4 - 7 January 2010, Orlando, Florida

AIAA 2010-353

Direct numerical simulation of hypersonic turbulent boundary layers with varying freestream Mach number

L. Duan*, I. Beekman†, M. P. Martín‡

In this paper, the effects of freestream Mach number on the statistics and large-scale structures in compressible turbulent boundary layers are investigated using direct numerical simulations(DNS). DNS of turbulent boundary layers with nominal freestream Mach number ranging from 3 to 8 are performed. The validity of Morkovin's scaling, strong Reynolds analogy, and Walz's equation are assessed. We find that many of the scaling relations used to express compressible boundary layer statistics in terms of incompressible boundary layers still hold for the range of freestream Mach number considered. Compressibility effects are enhanced with increasing freestream Mach number but remain insignificant, and the turbulence dissipation remains primarily solenoidal. Moreover, the variation of near-wall streaks, iso-surface of the swirl strength, and hairpin packets with freestream Mach numbers demonstrates that increasing freestream Mach number decreases the coherency of turbulent structures.

Nomenclature

M	Mach number, dimensionless
ρ	Density, kg/m^3
T	Temperature, K
δ	Boundary layer thickness, mm
θ	Momentum thickness, mm
δ^*	Displacement thickness, mm
u_τ	Friction velocity, m/s
H	Shape factor, $H = \delta^*/\theta$, dimensionless
Re_θ	Reynolds number, $Re_\theta \equiv \frac{\rho_\delta u_\delta \theta}{\mu_\delta}$, dimensionless
$Re_{\delta 2}$	Reynolds number, $Re_{\delta_2} \equiv \frac{\rho_\delta u_\delta \theta}{\mu_w}$, dimensionless
Re_τ	Reynolds number, $Re_\tau \equiv \frac{\rho_w u_\tau \delta}{\mu_w}$, dimensionless
Cf	Skin friction, dimensionless
Superscripts	
$+$	inner wall units
Subscripts	
δ	Boundary layer edge

I. Introduction

An essential part of the study for compressible turbulent boundary layers is to check the validity of Morkovin's hypothesis. The hypothesis, first proposed by Morkovin,[1] is that, at moderate free-stream Mach numbers ($M \leq 5$), dilatation is small and any differences from incompressible turbulence can be accounted for by mean variations of fluid properties. This is the basis for the van Driest transformation, a

*Graduate student, Department of Mechanical and Aerospace Engineering, Princeton University. Visiting student, Department of Aerospace Engineering, University of Maryland, College Park
†Graduate student, Department of Mechanical and Aerospace Engineering, Princeton University. Visiting student, Department of Aerospace Engineering, University of Maryland, College Park
‡Associate Professor, Department of Aerospace Engineering, University of Maryland

velocity scaling that accounts for the fluid-property variations to collapse compressible flow data onto the "universal" incompressible distribution. The check for validity of Morkovin's hypothesis consists primarily of experiments and numerical simulations at moderate Mach numbers.[2–4] Both experiments and numerical simulation confirmed that at moderate Mach numbers, the essential dynamics of the investigated supersonic turbulent boundary layers closely resemble the incompressible pattern under analogous conditions.

There are only limited studies for boundary layers at high Mach numbers. For example, one particularly important experiment was performed at Mach 6.7 at NASA Ames.[5–8] Similar measurements were done at Mach 7.2 by Baumgartner,[9] at Mach 11 by McGinley et al.,[10] and more recently at Mach 7.2 by Sahoo et al.[11] In terms of numerical simulations, Martin[12] performed direct numerical simulations (DNS) with freestream Mach number varying from 3 to 8. Maeder et al.[13] conducted DNS at Mach numbers 3, 4.5 and 6. Both previous experimental measurements and numerical simulations at high Mach numbers showed that the mean profile followed the standard semi-logarithmic profile when van Driest transformation is applied. Together these data support the notion that the scaling laws for the mean flow are essentially independent of Mach numbers.

However, the scaling with respect to turbulence behavior is still not so clear. Experimentally, two of the very few data sets on hypersonic turbulence measurements by Owen et al.[8] and McGinley et al.[10] showed that the turbulence intensities does not scale according to Morkovin. The data were taken by hot wire anemometry, and McGinley[10] observed that the data might suffered from poor frequency response and/or suspect calibrations of the hot wire anemometry used in the measurements. The more recent experiment by Sahoo et al.[11] for a flat-plat boundary layer at Mach 7.2 using Particle Image Velocimetry (PIV) also showed that the turbulence intensity does not follow Morkovin's scaling. However, the PIV data might also suffer from measurement errors due to low seeding density in high-speed flow. For the experimental observation that the turbulence intensities does not scale according to Morkovin, it is still not obvious whether it was due to the difficulties in experiments, or whether it was revealing new flow physics associated with high Mach number turbulence. Numerically, the DNS by Maeder et al.[13] showed that the compressible profiles of Reynolds stresses have a similar shape to the incompressible profiles, though they are fuller in the wake region for higher Mach numbers. However, as they mentioned, it remains to be assessed whether this is an artifact of their simulation caused by the relatively short domain. One purpose of the current study is to shed light on the above question by conducting direct numerical simulations (DNS) of turbulent boundary layers with a wide range of freestream Mach numbers to further analyze the scaling with respect to mean flow and turbulence behavior. In addition, more detailed turbulence statistics than turbulence intensities, such as strong Reynolds analogy(SRA) and turbulent kinetic energy budgets, will also be provided.

Besides turbulence statistics, another purpose of the current study is to investigate the effects of freestream Mach number on large scale coherent structures, since recent laboratory and numerical experiments indicate that large scale coherent structures play a key role in wall bounded turbulent flows at incompressible and compressible conditions.[14–20]

The paper are structured as follows. Flow conditions and simulation details are given in section II. Turbulence statistics are given in section III. Strong Reynolds analogy and turbulent kinetic energy budget are given in sections IV and V, respectively. Finally, structure analysis are given in section VI.

II. Simulation details

A. Flow conditions

To study Mach number effects, we use a DNS database of turbulent boundary layers[12,21] with nominal freestream Mach number ranging from 3 to 8. The boundary edge conditions and wall parameters for the DNS database are given in table 1, which provides freestream Mach number, density, and temperature, M_δ, ρ_δ, and T_δ, respectively, and boundary layer properties: momentum thickness, θ, shape factor, $H = \delta^*/\theta$ with δ^* the displacement thickness, boundary layer thickness δ, and different definitions of Reynolds number, where $Re_\theta \equiv \frac{\rho_\delta u_\delta \theta}{\mu_\delta}$, $Re_\tau \equiv \frac{\rho_w u_\tau \delta}{\mu_w}$, and $Re_{\delta 2} \equiv \frac{\rho_\delta u_\delta \theta}{\mu_w}$. For all cases, the wall condition is isothermal and prescribed to be nearly the adiabatic temperature.

To isolate the effect of varying freestream Mach number and study the effects of Mach number on turbulent boundary layer flow, it is desirable to match the Reynolds number of different Mach number cases. Here, we keep Re_τ and $Re_{\delta 2}$ nearly constant, with twofold on Re_θ across the cases.

Case	M_δ	ρ_δ(kg/m3)	T_δ(K)	$\frac{T_w}{T_\delta}$	Re_θ	Re_τ	$Re_{\delta 2}$	θ(mm)	H	δ(mm)
M3	2.99	0.0891	218.2	2.60	2605.8	421.5	1360.9	0.544	5.06	7.61
M4	3.98	0.0914	219.2	3.83	3407.2	405.7	1367.0	0.559	7.61	10.2
M5	4.97	0.0910	221.8	5.37	4086.4	425.4	1386.4	0.552	9.91	12.9
M6	5.93	0.0942	221.9	7.30	5163.3	387.1	1365.1	0.632	14.0	18.1
M7	6.94	0.0922	221.1	9.62	5574.0	357.5	1335.7	0.721	18.0	22.4
M8	7.80	0.0948	227.7	11.9	6817.2	344.5	1360.4	0.739	21.9	27.3

Table 1. Dimensional bounday layer edge and wall parameters for the DNS database

B. Numerical simulation parameters

Following Martin,[21] the computational domain size and grid resolution resolution are determined based on the characteristic large length scale, δ, and the characteristic small, near-wall length scale, z_τ, respectively. The computational domain must be large enough to contain a good sample of the large scales, while the grid resolution must be fine enough to resolve the near wall structures. The domain size ($L_x \times L_y \times L_z$), the grid size ($\Delta x \times \Delta y \times \Delta z$) and the number of grid points ($N_x \times N_y \times N_z$) are given in table 2. We take the streamwise, spanwise, and wall-normal directions to be x, y, and z, respectively. Uniform grids are used in the streamwise and spanwise directions as Δx^+ and Δy^+, where the superscript ($^+$) indicates scaling with inner, or wall values. Geometrically stretched grids are used in the wall-normal direction, with $z_k = z_2(\alpha^{k-1} - 1)/(\alpha - 1)$. The governing equations, numerical method, boundary conditions and initialization procedure are given in Martin.[21] The working fluid is air.

In the results that follow, both Reynolds and Favre averaging are used depending on simplicity of presentation and conventions used in the papers to which we are comparing. The Reynolds average f over the $x-$ and $y-$directions will be denoted by $\bar{f}$, or $< f >$, and fluctuations about this mean will be denoted by f'. The Favre average over the $x-$ and $y-$directions,$\tilde{f}$, is a density-weighted average:

$$\tilde{f} = \frac{\overline{\rho f}}{\overline{\rho}}.$$

Fluctuations about the Favre average will be denoted by f''.

Case	L_x/δ	L_y/δ	L_z/δ	Δx^+	Δy^+	z_2^+	α	N_x	N_y	N_z
M3	9.0	4.5	14.6	8.0	3.0	0.30	1.069	384	512	106
M4	7.9	2.0	15.4	7.4	2.8	0.30	1.069	384	256	114
M5	7.4	1.8	14.0	7.4	2.8	0.29	1.069	384	256	110
M6	7.0	1.7	15.3	7.2	2.7	0.30	1.069	384	256	114
M7	6.4	1.6	14.8	7.0	2.6	0.30	1.069	256	192	109
M8	6.0	1.5	15.6	6.8	2.5	0.27	1.069	256	192	106

Table 2. Grid resolution and domain size for the direct numerical simulations.

To assess the adequacy of the domain size, streamwise and spanwise two-point correlation for the streamwise velocity component, $R_{u'u'}$, are plotted. Figure 1(a,b) show that the streamwise and spanwise two-point correlations drop to zero for large separations for case M5. Similar results can be shown for other cases.

Figure 2 plots the energy spectrum at several wall normal locations for case M5. The energy distribution cascades down at least 8 orders of magnitude, indicating a good resolution of small scales. Similar results of energy spectrum can be obtained for other Mach number cases.

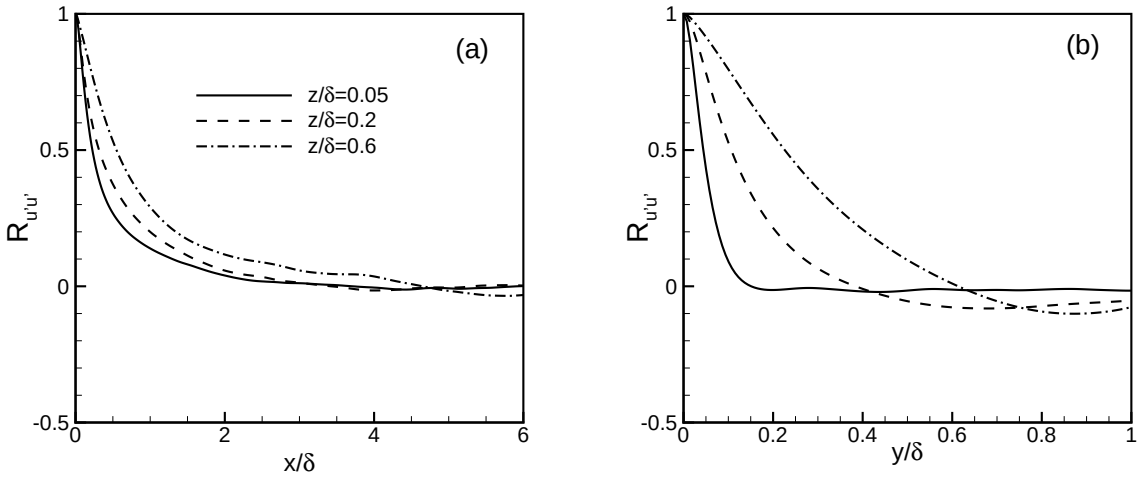

Figure 1. (a) Streamwise, and (b) spanwise two-point correlation for streamwise velocity component for M5

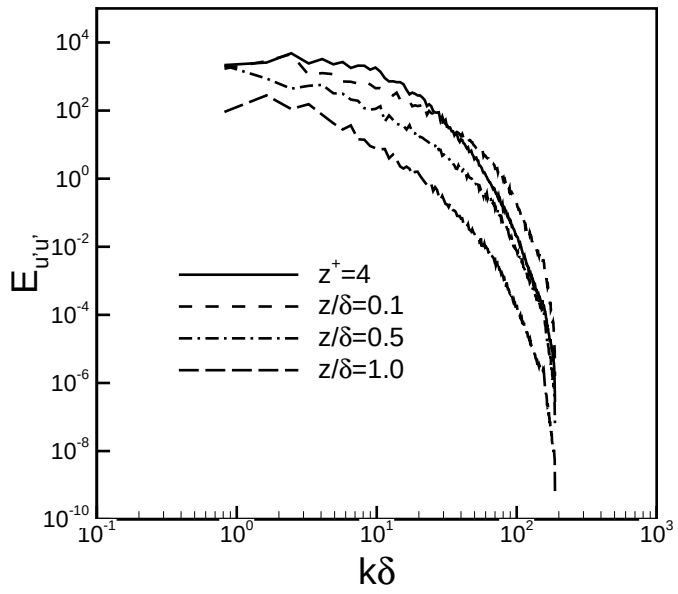

Figure 2. Two-dimensional energy spectra $E_{u'u'}$ at different wall normal locations for M5, where k is the wave number in streamwise-spanwise plane.

Another indication of the adequacy of the resolution is the value of $k_{max}\eta$, where k_{max} is the maximum wave number in x and η is the local Kolmogorov scale. The maximum and minimum of this value in current DNS are 2.8 and 0.6, respectively, which is adequate. For comparison, the DNS of a supersonic boundary layer at Mach 2.5 conducted by Guarini et al.[3] had values of 1.6 and 0.5 for the maximum and minimum of $k_{max}\eta$, respectively.

Further assessment of grid resolution near the wall can be conducted by comparing with DNS calculated skin friction C_f with well-established semi-empirical results. Table 3 gives the DNS calculated skin friction and the skin friction predicted by van Driest II theory.[22] It is shown that DNS calculated skin frictions are within 10% of the van Driest II prediction for all cases.

Case	C_f	$(C_f)_{VanDriest\Pi}$
M3	2.35×10^{-3}	2.14×10^{-3}
M4	1.83×10^{-3}	1.65×10^{-3}
M5	1.48×10^{-3}	1.35×10^{-3}
M6	1.17×10^{-3}	1.07×10^{-3}
M7	1.03×10^{-3}	9.67×10^{-4}
M8	8.43×10^{-4}	7.89×10^{-4}

Table 3. Skin friction of DNS database against that predicted by VanDriest Π theory[22] for different freestream Mach number cases

III. Turbulence statistics

For all cases, averages are computed over streamwise and spanwise directions of each field; then an ensemble average is calculated over fields spanning around one non-dimensional time unit. The time is non-dimensionalized by δ/u_τ, which corresponds to around $20\delta^*/u_e$. Using periodic boundary conditions in the streamwise direction during this period, the change in (δ, u_τ, Cf) is less than 5% and the flow can be view as a good approximation of a static station of a boundary layer.[23]

A. The turbulent Mach number

One convenient measure of the turbulent compressibility effects is the fluctuating Mach number, M', which is the RMS fluctuation of the Mach number. Another similar quantity is the turbulent Mach number, defined by

$$M_t = \frac{(\overline{u_i' u_i'})^{1/2}}{\overline{a}} \tag{1}$$

Morkovin[1] suggests that the turbulence is only weakly affected by compressibility if $M' \leq 0.2$ (0.3 according to Spina et al.[15] and Smits & Dussauge[24]). For adiabatic boundary layers, typically it is assumed that $M' = 0.3$ is reached when the freestream Mach number is 4 to 5.

Figure 3(a, b) plot the M_t and M', respectively. Both the M_t and M' increase with freestream Mach number. The peak value for M_t, figure 3(a), is about 0.29 and 0.4 for the freestream Mach 3 and 8 simulations. The fluctuating Mach number, figure 3(b), demonstrates a 'double peak' shape and has a more significant freestream Mach number dependence. Its maximum values of the first peak ranges from about 0.36 to 0.66.

B. Mean flow

Figure 4 plots the van Driest transformed velocity, $\bar{U}_{VD}$, for different Mach number cases. $\bar{U}_{VD}$ is defined as

$$\bar{U}_{VD} = \frac{1}{\bar{u}_\tau} \int_0^U (\overline{T_w}/\overline{T})^{1/2} dU \tag{2}$$

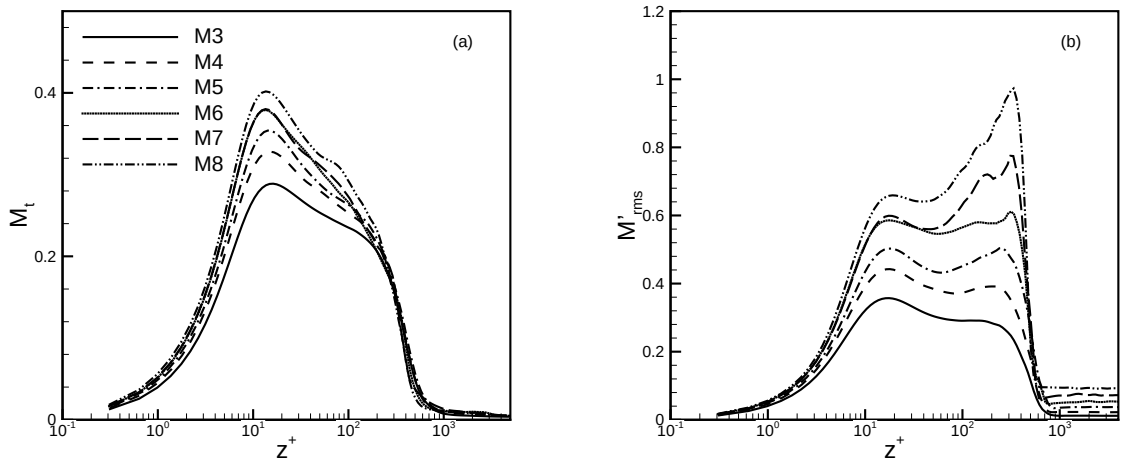

Figure 3. Simulation results of (a) turbulence Mach number and (b) fluctuating Mach number for cases with different freestream Mach number.

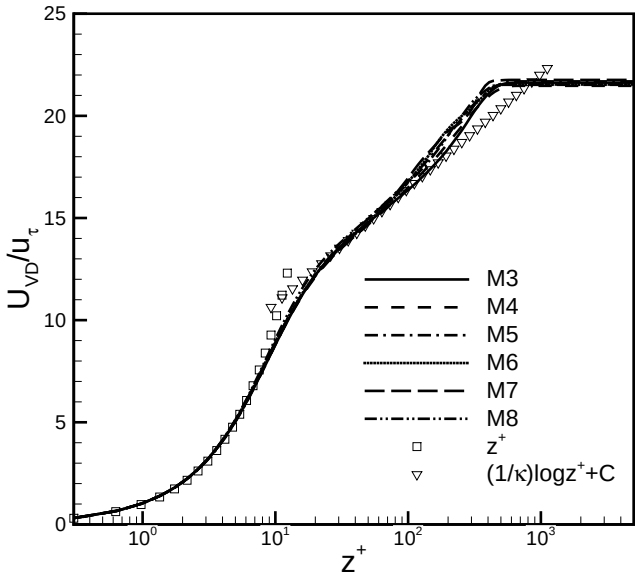

Figure 4. van Driest transformed velocity for different freestream Mach number cases

The profiles of $\bar{U}_{VD}$ for various Mach number cases collapse extremely well. The log-region is very well described by $(1/\kappa)logz^+ + C$ with $\kappa = 0.41$ and $C = 5.2$.

One of commonly used temperature-velocity relationships for zero pressure gradient boundary layers is Walz's equation:[25]

$$\frac{\bar{T}}{\bar{T}_\delta} = \frac{\bar{T}_w}{\bar{T}_\delta} + \frac{\bar{T}_r - \bar{T}_w}{\bar{T}_\delta}\left(\frac{\bar{u}}{\bar{u}_\delta}\right) + \frac{\bar{T}_\delta - \bar{T}_r}{\bar{T}_\delta}\left(\frac{\bar{u}}{\bar{u}_\delta}\right)^2 \tag{3}$$

Figure 5 shows the comparison between (3) and DNS results. It is shown that there is an excellent agreement for all the Mach number cases.

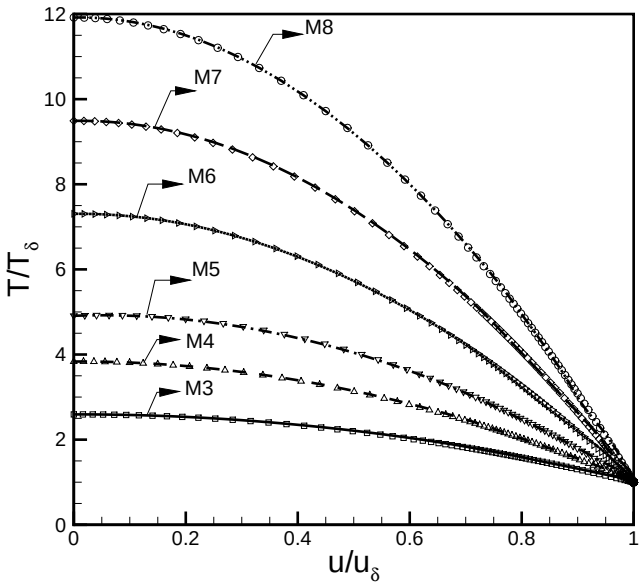

Figure 5. Test of Walz's equation, as expressed by (3) for cases with different freestream Mach number. Line: DNS; Symbol: Walz's relation given by (3).

C. Turbulence quantities

Figure 6(a d) plots density-weighted streamwise, spanwise and wall-normal components of velocity fluctuations as well as Reynolds shear stress normalized by wall shear stress. The streamwise velocity fluctuations of different Mach number cases are also compared with the incompressible results by Spalart.[26] It is shown that Morkovin's scaling largely collapse the data over the range of freestream Mach numbers considered. The compressible profiles have a similar shape to the incompressible profiles, and the compressible peak values are higher than the incompressible ones, as also observed by Gatski & Erlebacher[27] and Pirozzoli.[4]

It is important to notice that in Martin[21] the field is initialized using the Morkovin scaling to populate the velocity fluctuations and then the flow is allowed to evolve to a physical state, and we have checked the influence of different initializations on the final results. Figure 7(a) plots initial streamwise turbulence intensity, with and without assuming Morkovin scaling for velocity fluctuations, denoted as Case I and II, respectively. Figure 7(b) plots corresponding final converged physical results obtained from the two different initializations. The data show that the flow reaches the same physical state regardless of the initial condition, whereas the simulation transient to reach the physical state does depend on different initializations.

IV. Reynolds Analogies

Morkovin[1] proposed five SRA relations. Three of them are as follows:

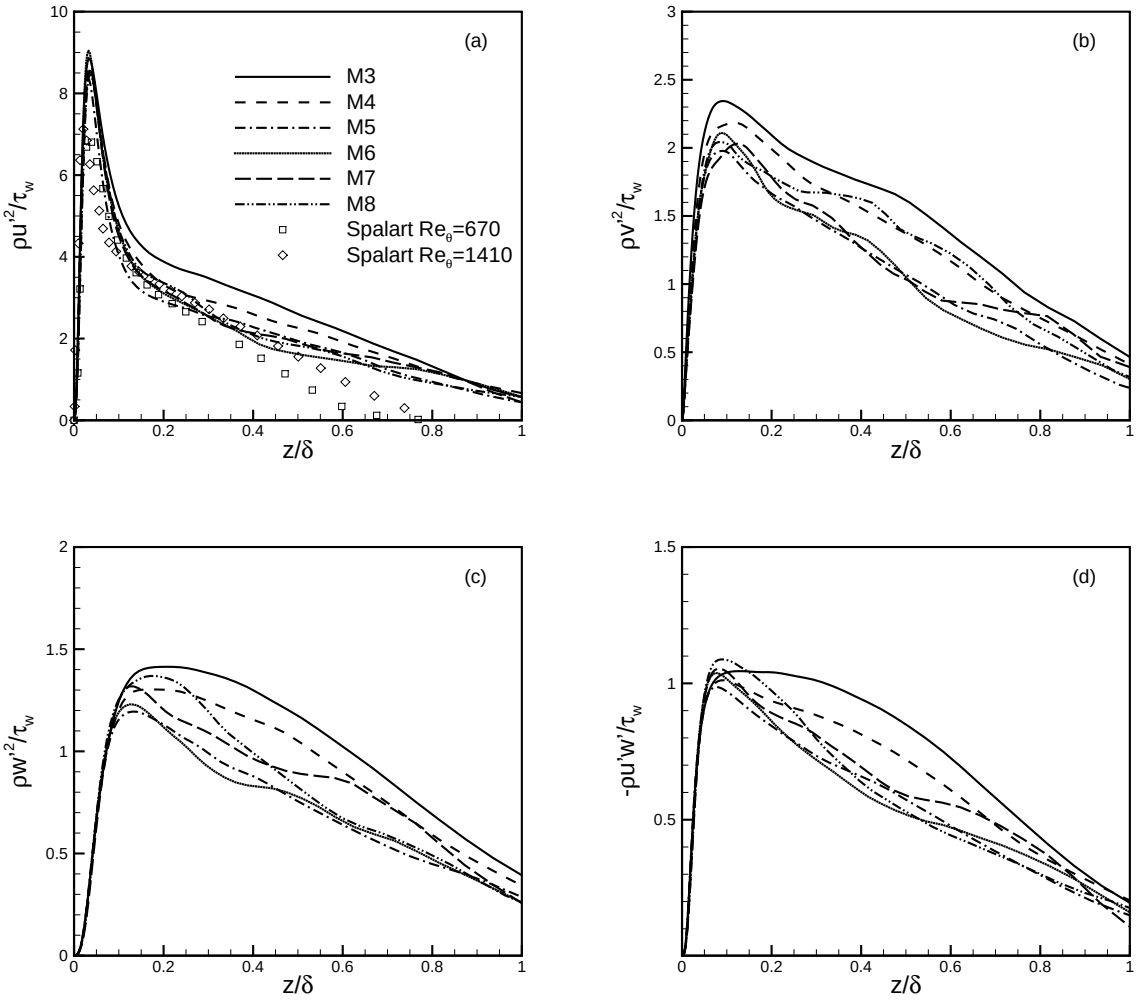

Figure 6. (a) **Steamwise,** (b) **spanwise,** (c) **wall-normal velocity fluctuations and** (d) **Reynolds shear stress for different freestream Mach number cases**

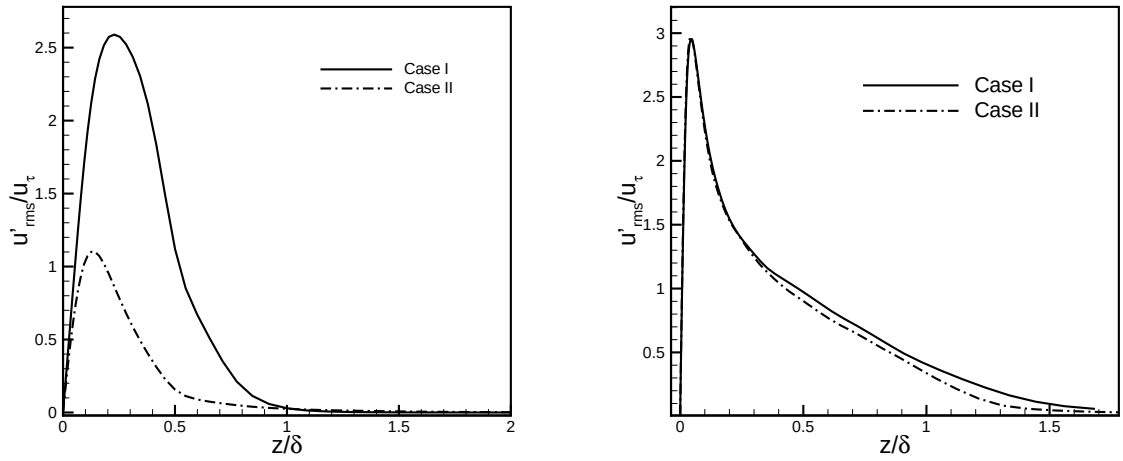

Figure 7. (*a*) Initial and (*b*) final converged streamwise turbulence intensity with and without assuming Morkovin scaling for velocity fluctuations for Mach 7.

$$\frac{T''_{RMS}/\tilde{T}}{(\gamma-1){M_a}^2(u''_{RMS}/\tilde{u})} \approx 1 \tag{4}$$

$$-R_{u''T''} \approx 1 \tag{5}$$

$$Pr_t = \frac{\overline{\rho u''w''}(\partial\tilde{T}/\partial z)}{\overline{\rho w''T''}(\partial\tilde{u}/\partial z)} \approx 1 \tag{6}$$

Figure 8 plots the relationship between RMS temperature and streamwise velocity fluctuations for different freestream Mach number cases. It is shown that (4) is nearly satisfied for $z/\delta < 0.6$ for all the Mach number cases, consistent with the DNS of adiabatic turbulent boundary layer given by Guarini et al.[3] and Martin.[21]

Figure 9 plots the correlation between temperature and velocity fluctuations across the boundary layer for different Mach number cases. It is shown that $-R_{u''T''}$ is not a strong function of freestream Mach number. Through most of the boundary layer, u'' and T'' are anti-correlated and $-R_{u''T''}$ is around 0.6, similar to the results reported by Guarini et al.[3]

Figure 10 plots turbulent Prandtl number across the boundary layer. Pr_t is insensitive to freestream Mach number condition and is close to unity in most of the boundary layer.

V. Turbulent kinetic energy budget

The turbulent kinetic energy is defined as:

$$\tilde{k} = \frac{1}{2}\frac{\overline{\rho u_i'' u_i''}}{\overline{\rho}} \tag{7}$$

and the budget equation for turbulent kinetic energy is, after assuming homogeneity in streamwise and spanwise directions, given by

$$\frac{\partial}{\partial t}(\overline{\rho}\tilde{k}) + \tilde{w}\frac{\partial}{\partial z}(\overline{\rho}\tilde{k}) = P + T + \Pi + \phi_{dif} + \phi_{dis} + ST \tag{8}$$

where

$$P = -\overline{\rho u_i'' w''}\frac{\partial \tilde{u}_i}{\partial z},$$

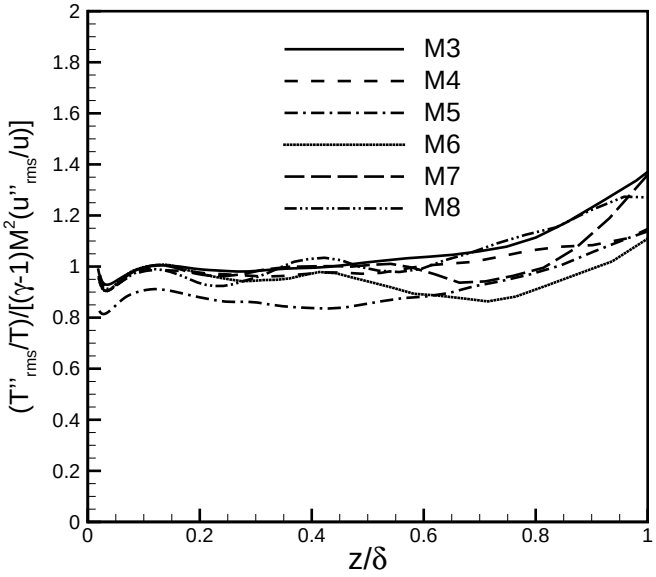

Figure 8. Test of the strong Reynolds analogy, as expressed by (4) for different freestream Mach number cases

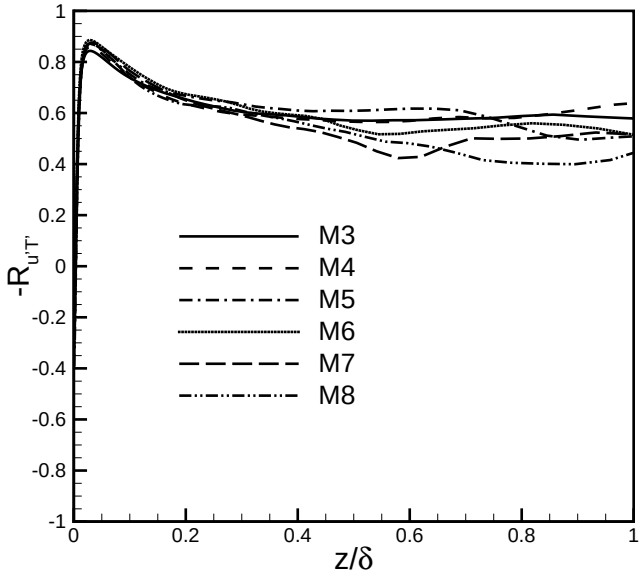

Figure 9. $-R_{u''T''}$ for cases with different freestream Mach number.

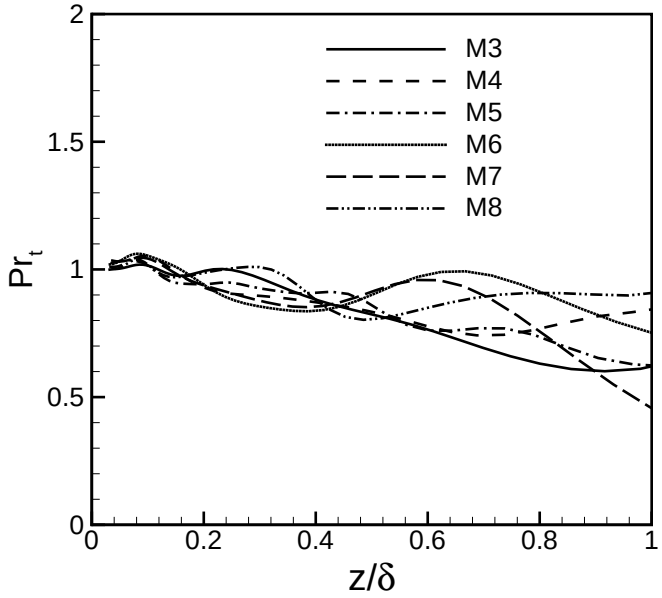

Figure 10. Pr_t **for cases with different freestream Mach numbers.**

$$
\begin{aligned}
T &= -\frac{1}{2}\frac{\partial}{\partial z}\overline{\rho u_i'' u_i'' w''}, \\
\Pi &= \Pi_t + \Pi_d = -\frac{\partial}{\partial z}\overline{w'' p'} + \overline{p'\frac{\partial u_i''}{\partial x_i}}, \\
\phi_{dif} &= \frac{\partial}{\partial z}\overline{u_i'' \tau_{iz}'}, \\
\phi_{dis} &= -\overline{\tau_{ij}'\frac{\partial u_i''}{\partial x_j}}, \\
ST &= -\overline{w''}\frac{\partial \overline{p}}{\partial z} + \overline{u_i''}\frac{\partial \overline{\tau_{ij}}}{\partial x_j} - \overline{\rho}\tilde{k}\frac{\partial \tilde{w}}{\partial z},
\end{aligned}
$$

The terms in (8) can be interpreted as follows: the left-hand side is the substantial derivative of the turbulent kinetic energy along a mean streamline; P is the rate of production of turbulent kinetic energy due to mean velocity gradient; T is turbulent transport; Π is the pressure terms (pressure diffusion and pressure dilatation, respectively); ϕ_{dif} is viscous diffusion; ϕ_{dis} is viscous dissipation; and ST represents terms that arise when the density is not constant. The first two appear due to the difference between the Favre and Reynolds averaging and the third term is the production term due to dilatation. Besides terms in ST, pressure dilatation as well as dilatational dissipation are also due to non-constant density.

Figure 11(a,b) plot the terms in the budget of turbulent kinetic energy, normalized by conventional wall variables (defined in terms of the mean density, viscosity and shear stress at the wall) and 'semi-local' scaling[28] (replacing $\overline{\rho}_w$ with $\overline{\rho}(z)$, u_τ with $u_\tau^* \equiv \sqrt{\tau_w/\overline{\rho}(z)}$, and $z_\tau^* \equiv \overline{\mu}(z)/(\overline{\rho}(z)u_\tau^*)$), respectively. ST is small and has not been included on the plot. It is shown that although TKE budget terms scale well in inner scaling, a better scaling is achieved when the data are scaled with local thermodynamic quantities.

Next, we study the influence of Mach number on pressure terms. There are three pressure terms: pressure diffusion (Π_t), pressure dilatation (Π_d), and compressibility (Π_c). The three terms are:

$$
\Pi_t = -\frac{\partial \overline{w'' p'}}{\partial z}, \quad \Pi_d = \overline{p'\frac{\partial u_i''}{\partial x_i}}, \quad \Pi_c = -\overline{w''}\frac{\partial \overline{p}}{\partial z} \tag{9}
$$

Of the three, Π_c and Π_d are associated with compressibility effects.

Figure 12(a,b) plot the pressure terms for different Mach number cases, normalized in inner wall units and 'semi-local' scaling, respectively. It is shown that pressure terms are considerably smaller compared

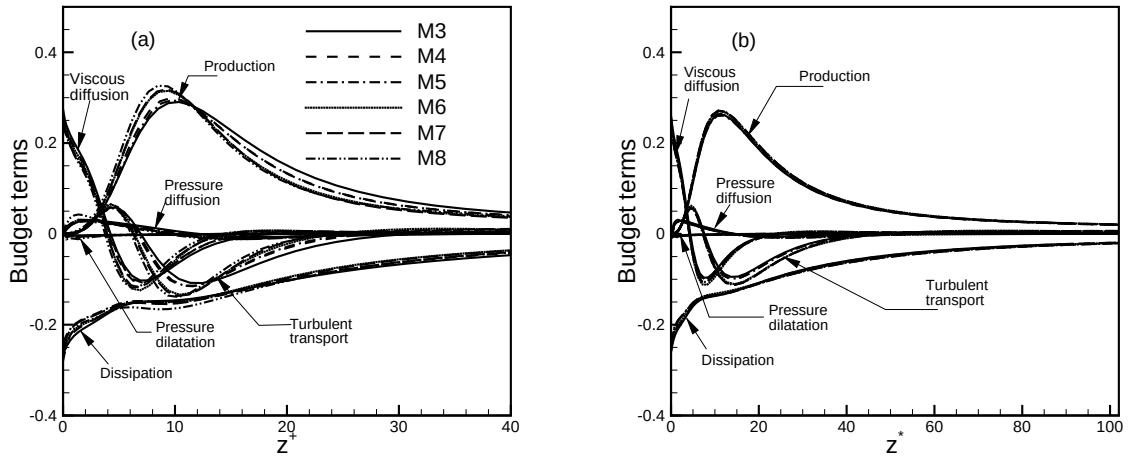

Figure 11. Turbulent kinetic energy budget for cases with different freestream Mach numbers, non-dimensionalized with (a) inner scale, and (b) semi-local units, respectively.

with production term and dissipation term in TKE budget. In both scalings, the magnitude of Π_d and Π_c increases as freestream Mach number increases, indicating stronger compressibility effects with increasing freestream Mach number. This trend is the direct outcome of the increase in M_t and M'_{rms} with increasing freestream Mach number, as it is shown in 3(a, b). Π_c goes to zero as it comes to the wall and is much smaller compared with Π_t and Π_d.

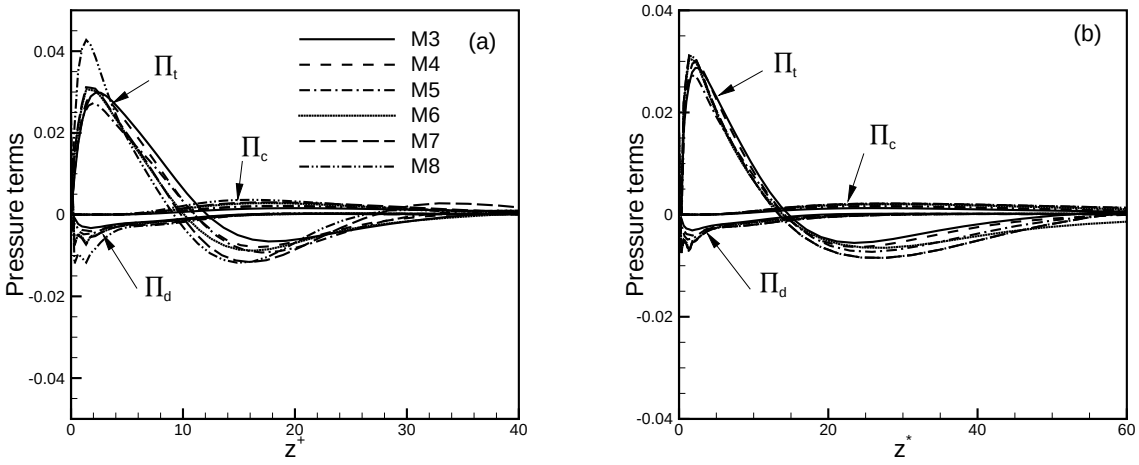

Figure 12. Π_t, Π_d, and Π_c for cases with different freestream Mach numbers, non-dimensionalized with (a) inner scale, and (b) semi-local units, respectively.

To study the effects of compressibility on the dissipation,[29,30] consider ϕ_{dis} which can be expressed as

$$\begin{aligned}\phi_{dis} &= \overline{\tau'_{ij}\frac{\partial u''_i}{\partial x_j}} = \overline{\tau'_{ij}\frac{\partial u'_i}{\partial x_j}} \\ &= \overline{\overline{\mu}\frac{\partial u'_i}{\partial x_j}\left(\frac{\partial u'_i}{\partial x_j}+\frac{\partial u'_j}{\partial x_i}-\frac{2}{3}\delta_{ij}\frac{\partial u'_k}{\partial x_k}\right)} \\ &+ \overline{\mu'\frac{\partial u'_i}{\partial x_j}\left(\frac{\partial u'_i}{\partial x_j}+\frac{\partial u'_j}{\partial x_i}-\frac{2}{3}\delta_{ij}\frac{\partial u'_k}{\partial x_k}\right)}\end{aligned}$$

$$+ \quad \overline{\mu' \frac{\partial u_i'}{\partial x_j}} \left(\frac{\partial \overline{u_i}}{\partial x_j} + \frac{\partial \overline{u_j}}{\partial x_i} - \frac{2}{3}\delta_{ij} \frac{\partial \overline{u_k}}{\partial x_k} \right). \tag{10}$$

where the three terms in this expression will be referred to as ϕ_1, ϕ_2, ϕ_3, respectively.

The terms, ϕ_2 and ϕ_3, which involve viscosity fluctuations, are negligible compared with ϕ_1. The first term, ϕ_1, can be further decomposed as follows:

$$\phi_1 = \overline{\mu}\overline{\omega_i'\omega_i'} + 2\overline{\mu}\left(\frac{\partial^2}{\partial x_i \partial x_i} \overline{u_j' u_j'} - 2\frac{\partial}{\partial x_i} \overline{u_j' \frac{\partial u_i'}{\partial x_j}} \right) + \frac{4}{3}\overline{\mu} \overline{\frac{\partial u_i'}{\partial u_i'} \frac{\partial u_k'}{\partial x_k}} \tag{11}$$

Where the first term on the right is the homogeneous incompressible dissipation, or the solenoidal part of dissipation, ϕ_s, the second term, ϕ_i, is due to inhomogeneity, and the third term, ϕ_d is due to dilatation.

Figure 13(a,b) plot ϕ_s, ϕ_i and ϕ_d for different Mach number cases, normalized in inner wall units and 'semi-local' scaling, respectively. For all Mach number cases, both dissipation due to dilatation and inhomogeneity are very small. Although dilatational dissipation increases slightly when increase the freestream Mach number, the Mach number condition influences the dissipation rate by mainly changing its solenoidal part.

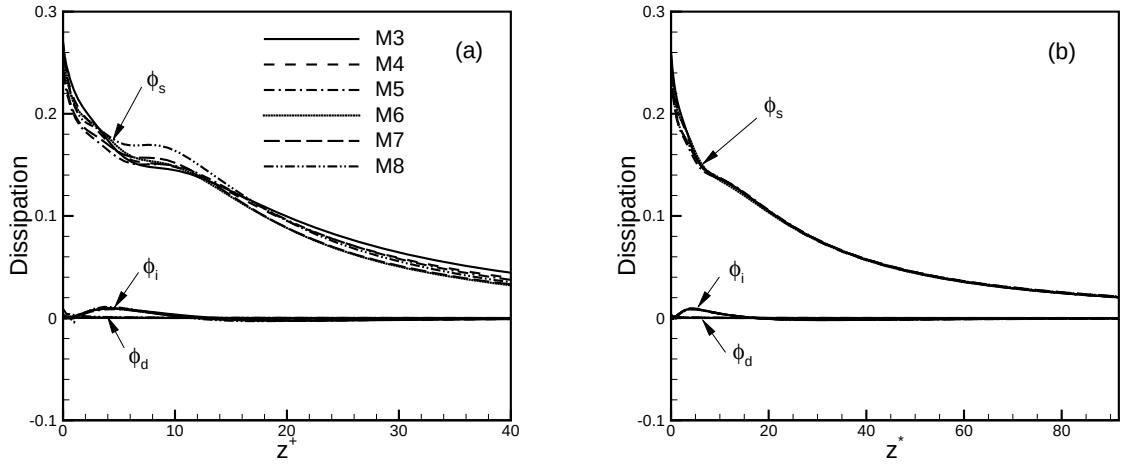

Figure 13. ϕ_s, ϕ_i, **and** ϕ_d **for different freestream Mach number cases, non-dimensionalized with (**a**) inner scale, and (**b**) semi-local units, respectively.**

The results and analysis given here show that at the Mach number range considered, although the freestream Mach number increases budget terms associated with compressibility effects, it influences the turbulent kinetic energy balance largely by quantitatively affecting terms that appear in the incompressible case.

VI. Structure analysis

A. Near-wall streaks

In this section, we investigate the effects of freestream Mach number on near-wall streaks. Figures 14(a,b) plot the instantaneous streamwise velocity fluctuations at $z^+ = 15$ for M3 and M8, respectively. Several occurrences of very long regions of negative u fluctuation are identified as streaks and are visible in the plots as elongated dark regions. It is also shown that there is a increase in spanwise meandering and decrease in the streamwise coherency for M8 compared with M3.

As far as the spanwise spacing of near-wall streaks is concerned, it is widely believed that the average spanwise spacing is about 100 viscous wall units for subsonic turbulent boundary layers.[31–33] For supersonic boundary layers, Ringuette et al.[34] showed that the average spanwise spacing is also about 100 viscous wall units, although it decreases when Mach number increases from 3 to 5. Table 4 gives the average spanwise

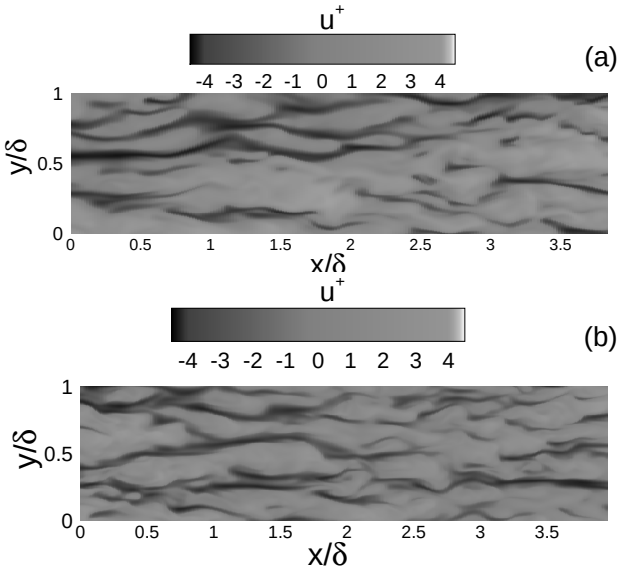

Figure 14. Instantaneous flow field at $z^+ = 15$ to visualize near-wall streaks for (a) M3 and (b) M8. Shading shows u fluctuations.

spacing of near-wall streaks at both $z^+ = 5$ and 15 in viscous wall units for different freestream Mach number cases. The velocity threshold used to determine spanwise streak spacing is $-0.1\overline{\rho u}(z)$.

At $z^+ = 5$, in general there is a decrease in the spanwise spacing with increasing freestream Mach number. For M3, the spanwise spacing is very similar to that of incompressible boundary layer and is very close to 100. From M3 to M8, there is approximately 26% decrease in spanwise streak spacing. At $z^+ = 15$, the trend with freestream Mach number is similar as $z^+ = 5$.

Case	$z^+ = 5$	$z^+ = 15$
M0	95.0	114.0
M3	91.2	98.5
M4	78.6	89.7
M5	75.3	84.1
M6	78.4	82.7
M7	71.5	75.4
M8	67.2	70.2

Table 4. Mean spanwise streak spacing in wall units for different freestream Mach number cases and incompressible flow results by Smith & Metzler[35] at $z^+ = 5$ and $z^+ = 15$

VII. Hairpin Vortices

In this section, we investigate the influence of freestream Mach number on large-scale coherent structures or hairpin vortices and packets. The vortical structures of boundary layers are demonstrated by using both iso-surfaces of swirl strength[36] and a correlation method after Brown & Thomas.[37]

Figures 15(a, b) plot iso-surfaces of the swirl strength for M3 and M8. It is shown that large scale hairpin vortices are observed for different Mach number cases, and the vortical structures become thinner and more chaotic with increasing freestream Mach number.

Next, hairpin vortices, packets and the corresponding low-momentum regions they encapsulate are inferred following Brown & Thomas[37] by correlating the wall shear stress, τ_w, at a single reference location

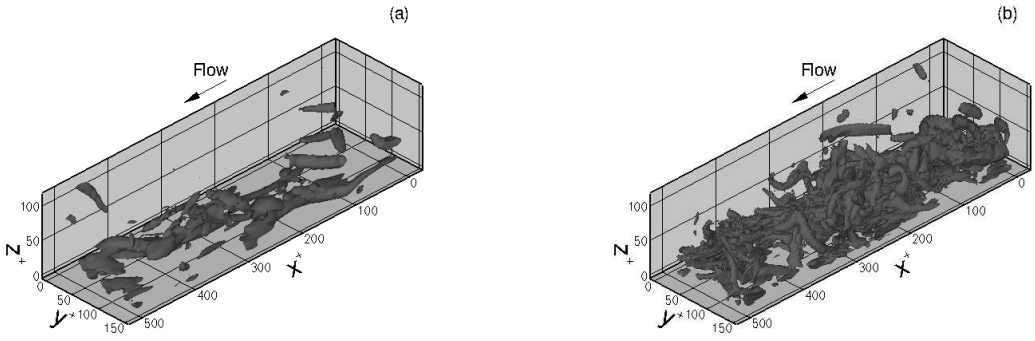

Figure 15. Iso-surface of λ_{ci} at $0.5\overline{\lambda_{ci}}$ to visualize voritcal structure for (a) M3 and (b) M8

with streamwise mass flux (ρu) at locations surrounding the reference point. The correlation coefficient is defined by

$$R_{\tau_w(\rho u)} = \frac{\overline{\tau'_w(x,y)(\rho u)'(x+\Delta x, y+\Delta y, \Delta z)}}{\tau'_{w,rms}(\rho u)'_{rms}} \tag{12}$$

Brown & Thomas[37] inferred the existence of coherent structures based upon experimentally obtained profiles of $R_{\tau_w(\rho u)}$ versus Δx at several wall normal locations; here with the complete DNS flow fields, we compute the three-dimensional distribution of $\overline{R}_{\tau_w(\rho u)}$ by simultaneously varying streamwise, spanwise, and wall normal separations of (ρu) and τ_w, thus a more direct visualization of structures can be obtained.

Figures 16(a,b) plot the three-dimensional distribution of $R_{\tau_w(\rho u)}$ for M3 and M8, respectively. For both cases, the streamwise, spanwise and wall normal width of viewing window are $-2\delta \leq \Delta x \leq 3\delta$, $-0.4\delta \leq \Delta y \leq 0.4\delta$ and $0.05 \leq \Delta z \leq 0.4\delta$, respectively, which are sufficient for the correlation to fall below 0.2. These plots show that for both cases, there is a positive region of $R_{\tau_w(\rho u)}$ in the middle surrounded by negative regions. This distribution of $R_{\tau_w(\rho u)}$ is directly related to the existence of hairpin vortices and packets. The positive region corresponds to low-momentum regions encapsulated by hairpin vortices or packets. Note the similarity in shape of this positive region with the region of induced low-speed fluid in the hairpin packet model of Adrian et al.[17] Between the legs of a hairpin vortex, the ejection of fluid causes negative $(\rho u)'$ and negative τ'_w, thus positive $R_{\tau_w(\rho u)}$. Outside the legs, the sweep events cause positive $(\rho u)'$, which correlates with the negative τ'_w between the legs to give negative $R_{\tau_w(\rho u)}$.

While both of these plots are strikingly similar to the conceptual model of Adrian et al.,[17] the stronger positive and negative values of the correlation coefficient for M3 compared with M8 indicate weaker, less coherent hairpin packets when the freestream Mach number is increased. The increased signature of the older, upstream packet in the M3 case is evidence of greater alignment, organization and interaction between hairpin packets.

The decreased organization of hairpin packets with increasing freestream Mach number can also be inferred by the average convection velocity of hairpin packets. Figure 17 plots the ratio of packet convection velocity to the mean flow velocty at different wall normal locations. The packet convection velocity is computed after Brown and Thomas by taking the conditional average of the streamwise velocity of points within each structure, as identified by $R_{\tau_w(\rho u)}$ exceeding a certain threshold.[38] The plot shows that there is a lag of packet convection velocity behind the mean, and the lag increases with decreasing freestream Mach number. The relatively slower convection velocity of hairpin packets most likely indicates that the hairpin vortices of the packets are more intense, more organized, or both, and therefore produce a relatively stronger back-flow that retards the overall packet velocity.

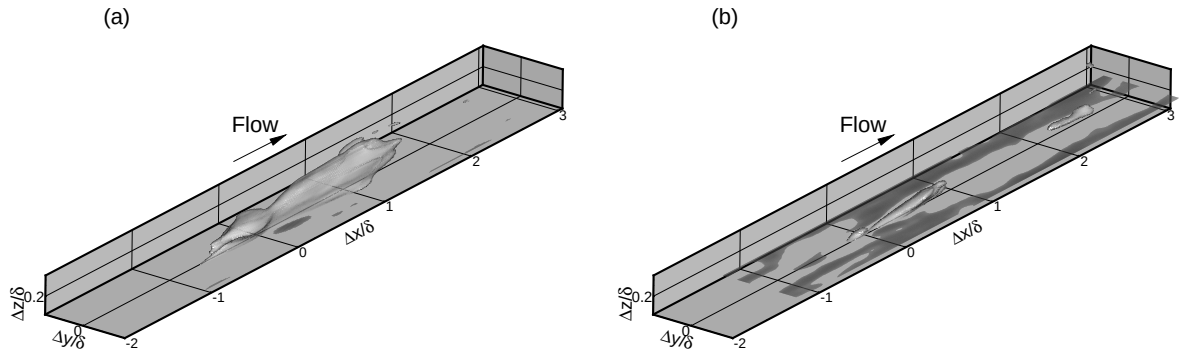

Figure 16. Iso-surfaces of $R_{\tau_w(\rho u)}$ to visualize vortical structure for (a) M3 and (b) M8. Iso-surface values at 0.13 (light) and -0.02 (dark) are plotted

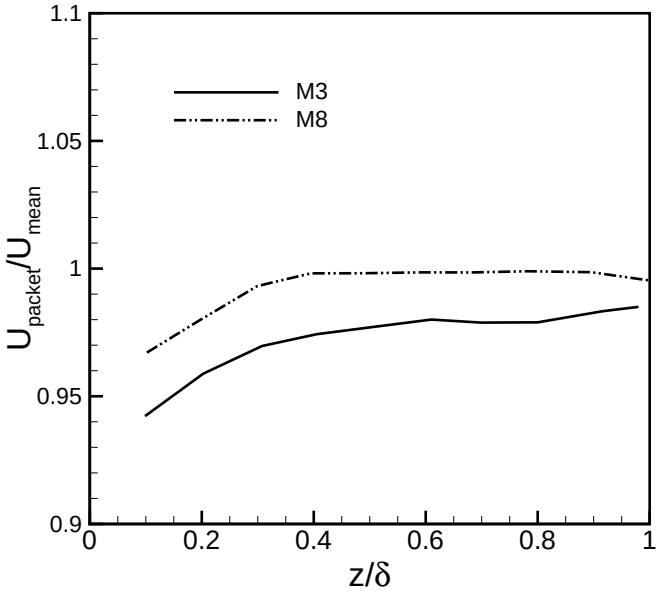

Figure 17. Ratio of average packet convection velocity to the mean flow velocity versus distance from the wall with the packet convection velocity.

VIII. Conclusion

We perform direct numerical simulations of turbulent boundary layers with freestream Mach number from 3 to 8 to study the effects of Mach number on boundary layer flow. It was shown that many of the scaling relations used to express compressible boundary layer statistics in terms of incompressible boundary layers also hold for the Mach number range considered. In particular, we have shown that the van Driest transformed velocity collapse different freestream Mach results with incompressible results; It is also shown that the RMS velocity fluctuations of different Mach numbers collapse by the mean density scaling suggested by Morkovin.

In terms of strong Reynolds analogy, it is shown that (4) is valid. The correlation between temperature and velocity fluctuations collapses for the Mach number cases considered and the values are smaller compared with experimental results.

The turbulent kinetic energy budget was calculated and compared for all the Mach number cases. It was shown that TKE budget terms collapse well when scaled with inner scaling.

The profiles of M_t, M'_{rms} show that compressibility effects increase with increasing freestream Mach number. However, terms arising from the non-vanishing velocity-divergence in TKE budgets, such as pressure dilatation and dilatational dissipation, remain small. and the freestream Mach number influences the turbulent kinetic energy largely by affecting the terms that appear in the incompressible case.

Increasing the freestream Mach number has the effect of increasing the apparent chaos of the turbulent structures. We have seen that the near-wall streaks become less coherent with increasing freestream Mach number. In addition, with increasing freestream Mach number vortical structures become thinner and more chaotic, as shown in figure 15. The strength of and organization between hairpin packets, appears to decrease with increasing freestream Mach number, as shown by the iso-surface of $R_{\tau_w(\rho u)}$ and the average convection velocity of packets.

IX. Acknowledgment

This work is supported by NASA under Grant NNX08ADO4A.

References

[1]Morkovin, M. V., "Effects of compressibility on turbulent flows," *In Mécanique de la Turbulence*, Vol. NRS, 1962, pp. 367–380.

[2]Fernholz, H. H. and Finley, P. J., "CRITICAL COMMENTARY ON MEAN FLOW DATA FOR TWO-DIMENSIONAL COMPRESSIBLE TURBULENT BOUNDARY LAYERS." *AGARDograph*, , No. 253, 1980.

[3]Guarini, S. E., Moser, R. D., Shariff, K., and Wray, A., "Direct numerical simulation of a supersonic turbulent boundary layer at Mach 2.5," *J. Fluid Mech.*, Vol. 414, 2000, pp. 1–33.

[4]Pirozzoli, S., Grasso, F., and Gatski, T. B., "Direct numerical simulation and analysis of a spatially evolving supersonic turbulent boundary layer at M = 2.25," *Physics of Fluids*, Vol. 16, No. 3, 2004, pp. 530–545.

[5]Mikulla, V. and Horstman, C., "Turbulence measurements in hypersonic shock-wave boundary-layer interaction flows," *AIAA Journal*, Vol. 14, No. 5, 1976, pp. 568–575.

[6]Owen, F. and Horstman, C., "On the structure of hypersonic turbulent boundary layers," *Journal of Fluid Mechanics*, Vol. 53, 1972, pp. 611–636.

[7]Owen, F. and Horstman, C., "Turbulent properties of a compressible boundary layer," *AIAA Journal*, Vol. 10, No. 1, 1972, pp. 1418–1424.

[8]Owen, F., Horstman, C., and Kussoy, M., "Mean and fluctuating flow measurements on a fully-developed non-adiabatic hypersonic boundary layer," *Journal of Fluid Mechanics*, Vol. 70, 1975, pp. 393–413.

[9]Baumgartner, M., *Turbulence structure in a hypersonic boundary layer*, Ph.D. thesis, Princeton University, Princeton, 1997.

[10]McGinley, C., Spina, E., and Sheplak, M., "Turbulence measurements in a Mach 11 helium turbulent boundary layer," *AIAA Paper*, Vol. 94-2364, 1994.

[11]Sahoo, D., Schultze, M., and Smits, A., "Effects of roughness on a turbulent boundary layer in hypersonic flow," *AIAA Paper*, Vol. 2009-3678, 2009.

[12]Martin, M. P., "DNS of hyersonic turbulent boundary layers," *AIAA Paper*, Vol. 2004-2337, 2004.

[13]Maeder, T., Adams, N. A., and Kleiser, L., "Direct simulation of turbulent supersonic boundary layers by an extended temporal approach," *Journal of Fluid Mechanics*, Vol. 429, 2001, pp. 187–216.

[14]Robinson, S. K., "Coherent motions in the turbulent boundary layer," *Anuu. Rev. Fluid Mech.*, Vol. 23, 1991, pp. 601–639.

[15]Spina, E. F., Smits, A. J., and Robinson, S. K., "The physics of supersonic turbulent boundary layers," *Annu. Rev. Fluid Mech.*, Vol. 26, 1994, pp. 287–319.

[16]Kim, K. C. and Adrian, R. J., "Very large-scale motion in the outer layer," *Physics of Fluids*, Vol. 11, No. 2, 1999, pp. 417–422.

[17]Adrian, R., Meinhart, C., and Tomkins, C., "Vortex organization in the outer region of the turbulent boundary layer," *Journal of Fluid Mechanics*, Vol. 422, 2000, pp. 1–54.

[18]Ganapathisubramani, B., Clemens, N., and Dolling, D., "Large-scale motions in a supersonic turbulent boundary layers," *Journal of Fluid Mechanics*, Vol. 556, 2006, pp. 1–11.

[19]Hutchins, N. and Marusic, I., "Evidence of very long meandering features in the logarithmic region of turbulent boundary layers," *Journal of Fluid Mechanics*, Vol. 579, 2007, pp. 1–28.

[20]Ringuette, M. J., Wu, M., and Martin, M. P., "Coherent structures in direct numerical simulation of turbulent boundary layers at Mach 3," *Journal of Fluid Mechanics*, Vol. 594, 2008, pp. 59–69.

[21]Martin, M. P., "Direct numerical simulation of hypersonic turbulent boundary layers. Part 1. Initialization and comparison with experiments," *Journal of Fluid Mechanics*, Vol. 570, 2007, pp. 347–364.

[22]van Driest, E. R., "The problem of aerodynamic heating," *Aeronautical Engineering Review*, Vol. 15, No. 10, 1956, pp. 26–41.

[23]Xu, S. and Martin, M. P., "Assessment of inflow boundary conditions for compressible turbulent boundary layers," *Physics of Fluids*, Vol. 16, No. 7, 2004, pp. 2623–2639, Cited By (since 1996): 17.

[24]Smits, A. J. and Dussauge, J. P., *Turbulent shear layers in supersonic flow*, American Institute of Physics, 2nd ed., 2006.

[25]Walz, A., *Boundary Layers of Flow and Temperature*, MIT Press, 1969.

[26]Spalart, P. R., "DIRECT SIMULATION OF A TURBULENT BOUNDARY LAYER UP TO Re_θ equals 1410." *Journal of Fluid Mechanics*, Vol. 187, 1988, pp. 61–98.

[27]Gatski, T. B. and Erlebacher, G., "Numerical simulation of a spatially evolving supersonic turbulent boundary layer," Tech. Rep. 211934, NASA Tech. Memo., 2002.

[28]Huang, P. G., Coleman, G., and Bradshaw, P., "Compressible turbulent channel flows: DNS results and modelling," *Journal of Fluid Mechanics*, Vol. 305, 1995, pp. 185–218.

[29]Zeman, O., "Dilatation dissipation: The concept and application in modeling compressible mixing layers," *Physics of Fluids A*, Vol. 2, No. 2, 1990, pp. 178–188, Cited By (since 1996): 103.

[30]Sarkar, S., Erlebacher, G., Hussaini, M. Y., and Kreiss, H. O., "Analysis and modelling of dilatational terms in compressible turbulence," *Journal of Fluid Mechanics*, Vol. 227, 1991, pp. 473–493.

[31]P. S. Runstadler, S. J. K. and Reynolds, W. C., "An experimental investigation of flow structure of the turbulent boundary layer," Tech. rep., Mechanical Engineering Department, Stanford University, 1963.

[32]Kline, S. J., Reynolds, W. C., Schraub, F. A., and Runstaller, W. P., *Journal of Fluid Mechanics*, Vol. 30, 1967, pp. 741–773.

[33]Bakewell Jr., H. P. and Lumley, J. L., "Viscous sublayer and adjacent wall region in turbulent pipe flow," *Physics of Fluids*, Vol. 10, No. 9, 1967, pp. 1880–1889.

[34]Ringuette, M., Martin, M., Smits, A., and Wu, M., "Characterization of the Turbulence Structure in Supersonic Boundary Layers Using DNS Data," *AIAA Paper*, Vol. 2006-3539, 2006.

[35]Smith, C. R. and Metzler, S. P., "CHARACTERISTICS OF LOW-SPEED STREAKS IN THE NEAR-WALL REGION OF A TURBULENT BOUNDARY LAYER." *Journal of Fluid Mechanics*, Vol. 129, 1983, pp. 27–54.

[36]Zhou, J., Adrian, R. J., Balachandar, S., and Kendall, T. M., "Mechanisms for generating coherent packets of hairpin vortices in channel flow," *Journal of Fluid Mechanics*, Vol. 387, 1999, pp. 353–396.

[37]Brown, G. L. and Thomas, A. S. W., "Large structure in a turbulent boundary layer," *Physics of Fluids*, Vol. 20, No. 10, 1977, pp. S243–S252.

[38]O'Farrell, C. and Martin, M., "Chasing eddies and their wall signature in DNS data of turbulent boundary layers," *accepted for publication in Journal of Turbulence*, 2009.